

Quantification of the Adsorption Kinetics of a Model Corrosion Inhibitor on Gold Using QCM-D

Kushal Singla,^{*} Hubert Perrot,^{‡,**} Bruce Brown,^{*} and Srdjan Nešić^{‡,*}

In the present study, a quartz crystal microbalance with dissipation monitoring (QCM-D) was used to investigate the adsorption of a model corrosion inhibitor compound, tetradecyldimethylbenzylammoniumbromide (BDA-C14), on gold electrode. Sauerbrey's equation was used to analyze the equilibrated normalized frequency change for estimation of the adsorbed mass and adsorbed layer thickness at different bulk inhibitor concentrations after careful validation. The average adsorbed layer thickness for BDA-C14 at tested experimental conditions lie in the range of 1 nm to 1.4 nm. Time-dependent part of the frequency change was analyzed using Langmuir adsorption isotherm to calculate the kinetic constants ($k_A = 0.075 \pm 0.02 \text{ mM}^{-1} \text{ s}^{-1}$, $k_D = 0.0023 \pm 0.0007 \text{ s}^{-1}$, and $K_{AD} = 32.2 \text{ mM}^{-1}$). Equilibrium surface coverage (θ_{eq}) was estimated at each bulk inhibitor concentration tested: 0.69 for 25 ppm(w), 0.74 for 50 ppm(w), and 0.91 for 100 ppm(w). Some theoretical calculations are also shown explaining the use of known molecular geometry and adsorption kinetics information from QCM-D analysis to reasonably speculate the predominant adsorbed layer configuration. A conscious effort is made to state and validate each assumption made for the analysis of the experimental results.

KEY WORDS: adsorption kinetics, corrosion inhibitors, Langmuir adsorption isotherm, quartz crystal microbalance with dissipation monitoring, quaternary ammonium, surface coverage

INTRODUCTION

Oil and gas transportation pipelines are often prone to internal corrosion in service environments. Corrosion-related accidents pose severe risks to human life, cause significant economic losses amounting to hundreds of billions of dollars annually, and lead to environmental damage causing costly ruptures and spills that endanger lives and contaminate ecosystems. Combating these issues requires rigorous inspections, corrosion-resistant materials, advanced coatings, and chemical treatments to enhance pipeline safety and integrity. Among various strategies used to combat the problem of internal corrosion in oil and gas transportation pipelines, corrosion mitigation using inhibitors, especially organic corrosion inhibitors, is a favorable choice because of better economic feasibility and moderately low toxicity.¹⁻³ Organic corrosion inhibitors are typically surfactant-type organic molecules with a hydrophilic head group that adsorbs to the corroding metal surface and a hydrophobic alkyl tail which forms a hydrophobic barrier between the metal and the corrosive environment. Hence, the adsorption of inhibitor molecules on the metal substrate reduces the reaction rates and protects against corrosion.⁴⁻⁸

Inhibition phenomena have been studied extensively using various electrochemical techniques, but due to the intrinsic limitations associated with traditional electrochemical techniques, the data collected can only provide an indirect estimate of the amount and rate of the inhibitor adsorption.^{6,9-14}

To correlate corrosion rate measurements with inhibitor adsorption on the metal surface, certain assumptions must be made such as assuming a linear relationship between the reduction in corrosion rates and the extent of inhibitor adsorption, as described by the geometric blockage model. The validity of such assumptions remains uncertain and hence inferring adsorption behavior from electrochemical measurements can be ambiguous. Measurement of steady-state corrosion rates using the linear polarization resistance (LPR) technique has been previously applied for model inhibitor compounds to study the inhibitor adsorption phenomenon.^{7,9-11,15-20} However, for the LPR technique, a minimum time step is needed between two corrosion measurements for the system to stabilize and equilibrate. If this time step between corrosion measurements exceeds the time required for the inhibitor adsorption process to equilibrate, then the important kinetics information will be lost between two corrosion rate measurements and hence the measured corrosion rate data may not be suitable for quantification of the adsorption kinetics. There is a lack of molecular-level understanding of electrode/electrolyte interfacial properties such as adsorbed layer thickness, orientation of adsorbed inhibitor molecules, and kinetics of adsorption in the presence of corrosion inhibitors, hence the exact adsorption mechanisms are not clearly understood.⁹⁻¹⁰ So, in designing inhibitor molecules with improved efficiency and to have a better understanding of underlying inhibition mechanisms, it becomes extremely important to study and quantify adsorption mechanisms independently. The present research used a

Submitted for publication: August 13, 2024. Revised and accepted: October 23, 2024. Preprint available online: October 24, 2024, <https://doi.org/10.5006/4634>.

[‡] Corresponding authors. E-mail: hubert.perrot@sorbonne-universite.fr; nesic@ohio.edu.

^{*} Institute for Corrosion and Multiphase Technology, Department of Chemical & Biomolecular Engineering, Ohio University, 342 West State Street, Athens Ohio 45701.

^{**} Sorbonne Université, CNRS, Laboratoire Interfaces et Systèmes Electrochimiques (LISE, UMR 8235), 4, place Jussieu, (case courrier 133), F-75005, Paris, France.

gravimetric sensor-quartz crystal microbalance with dissipation monitoring (QCM-D), capable of measuring a continuous mass change with respect to time to study the adsorption kinetics of a quaternary ammonium-based model corrosion inhibitor compound, tetradecyldimethylbenzylammonium bromide (BDA-C14), on gold-coated quartz crystal resonator (QCR).

The quartz crystal microbalance (QCM) is a powerful bulk acoustic wave sensor that can be effectively used to study surface reactivity.²¹ As QCM is a highly sensitive technique for changes on a substrate surface, sensitive to mass changes in the nanogram range, this method has found application in experimental studies focusing on corrosion inhibitor molecules adsorption on metal surfaces.²²⁻³² In principle, Sauerbrey's equation can be applied directly to convert the measured change in frequency to mass change on the QCR surface.^{21,33} With various assumptions associated with the development of Sauerbrey's equation, it holds well for gas phase measurements for quantitative analysis of mass change at QCR surface but for application of Sauerbrey's equation to in situ solution phase measurements; the validity of Sauerbrey's equation should be established.^{21,34-35} Ding in his Ph.D. dissertation has reported the use of QCM to study the adsorption of imidazoline-type corrosion inhibitors and explicitly acknowledged the troubles while converting directly the frequency change to mass change using Sauerbrey's equation.²² Karpovich, et al., discuss the adsorption kinetics of alkane-thiolate on gold surface measured using QCM.²³⁻²⁴ The authors successfully demonstrate the methodology to quantify the rate of monolayer growth from QCM measurements but refrain from reporting the absolute mass change associated with the formation of monolayer.²³⁻²⁴ By analyzing dissipation change, ΔD , in conjunction with frequency change, the use of Sauerbrey's equation was validated in the experimental system for quantitative results.³⁶⁻³⁸ With a QCM-D capable of simultaneous frequency and dissipation measurements conducted at multiple overtones, it can now be used to characterize the mechanical properties of the adsorbed layer.³⁶

Atomic force microscopy (AFM) has also found an application in direct imaging of adsorbed layers on various active and noble substrates.^{14,39-43} Previous AFM studies with quaternary ammonium-type surfactants have provided valuable insights into the structure of the adsorbed layer and thickness of the adsorbed layer on mica surfaces.^{14,42-43} With different modes available to use in AFM, it can also provide information on the properties of the surface such as adhesion, stiffness, and elasticity.⁴⁴ With QCM-D, dissipation response at multiple overtones can help in estimating the viscoelastic response of the adsorbed layer. So, the experimental results from these two techniques can be compared for a similar experimental system.⁴⁴ Moreover, virtually all AFM examinations have been performed on adsorbed layer surfaces that were formed before AFM examination, which lacks information about the time resolution and kinetics of adsorption.²³ Even the in situ AFM measurements provide only qualitative insights related to the adsorption of molecules on the substrate surface.¹⁴ The use of a QCM-D provides a viable means for the examination of adsorption and desorption kinetics at the electrode/electrolyte interface. Thus, with QCM-D, we have measured the rate at which adsorption happens in real time and the equilibrium adsorbed layer thickness was estimated. These measurements were compared to the values reported by Wang, et al., using AFM for the BDA-C14 model compound.¹⁴

In addition to experimental techniques, more recently, molecular simulations, both coarse grain and atomistic are used to study the adsorption behavior of surfactants. Molecular

simulation results for quaternary ammonium-based surfactants on gold substrates provide indications about the effect of the structure of molecules and intermolecular hydrophobic interactions on the nature and morphology of the adsorbed layer.^{14,45-49} The equilibrium structure data from these molecular simulations results reported in various publications for similar molecules was used and discussed in the present research to verify the assumptions made in QCM-D data analysis.⁴⁹

In this research, a QCM-D equipped with a flow control unit was used for the characterization of the electrode/electrolyte interface. More precisely, to better understand the nature of the adsorbed layer and quantify the adsorption kinetics of a model inhibitor compound, BDA-C14, on a noble metal substrate, gold electrode in 1 wt% NaCl solution. Adsorption experiments with BDA-C14 are reviewed for three bulk inhibitor concentrations: 25 ppm(w) [0.5 CMC, 0.0625 mM], 50 ppm (w) [1 CMC, 0.125 mM], and 100 ppm(w) [2 CMC, 0.25 mM]; where CMC refers to critical micelle concentration. Based on the QCM-D frequency changes and dissipation changes vs. time, experimental results are discussed for adsorbed mass, adsorbed layer thickness, surface coverage, and adsorption/desorption kinetic constants.

EXPERIMENTAL PROCEDURES

2.1 | Synthesis of Corrosion Inhibitor Model Compounds

Model corrosion inhibitor compounds were synthesized at the Institute for Corrosion and Multiphase Technology (ICMT) so that research could be conducted using known molecular structures and known purity levels for various single-molecule corrosion inhibitors.^{7,9,15-16} The rationale for using lab-synthesized compounds is to decrease the number of unknowns in experiments because it is understood that commercial inhibitor packages are mixtures of various molecules and contain formulations that are trade secrets.¹ The stable molecular structure and molecular mass of the adsorbed molecules are known in the present research enabling us to analyze experimental data for the adsorbed layer thickness and the orientation of the adsorbed species using the QCM-D.

For this work, a quaternary ammonium-type model inhibitor compound, named BDA-C14, was synthesized. BDA-C14 consists of a polar head group, dimethylbenzylammonium, and a hydrophobic tail comprised of 14 carbon atoms ($-C_{14}H_{29}$) as shown in Figure 1. The detailed synthesis procedure and reactions for BDA-C14 are described by Moradighadi, et al. The synthesized reaction product was characterized using proton

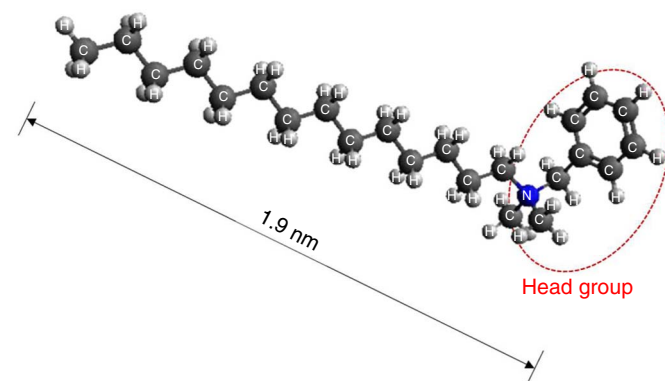


FIGURE 1. Molecular structure of tetradecyldimethylbenzylammonium (BDA-C14).⁵⁰

magnetic resonance and it was shown that the synthesized reaction product was recovered at 99% purity level.⁷

2.2 | Materials and Solution

AT-cut gold-coated, polished quartz crystals with a fundamental resonance frequency of ~5 MHz were used as the

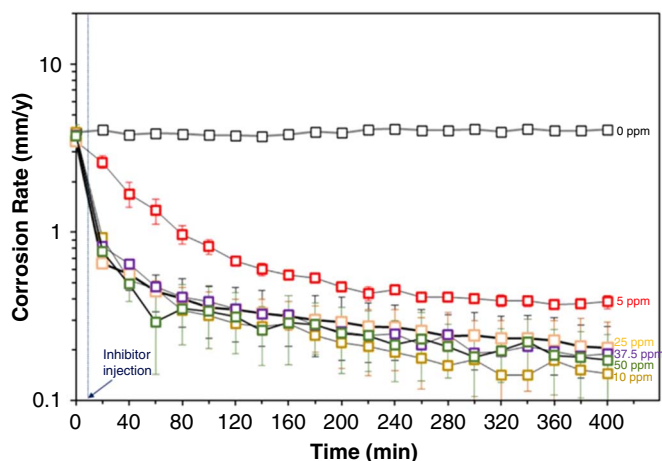


FIGURE 2. Electrochemical corrosion rate measurements with respect to time to determine metal surface saturation concentration of BDA-C14 model inhibitor compound in 1 wt% aqueous NaCl solution, 1 bar CO_2 , pH 4, and 30°C. Inhibitor addition in the solution phase (Reprinted with permission from.⁸ Copyright 2024 AMPP.)

Parameter	Value
Base electrolyte	1 wt% NaCl in deionized water
Inhibitor solution	25, 50, & 100 ppm(w) BDA-C14 in base electrolyte
Substrate/QCR	5 MHz, wrapped around configuration, Au/Ti, polished
Operating overtones	$n = 1, 3, 5, 7, 9, 11, \text{ and } 13$
Flow rate	0.05 mL/min

substrate for each experiment.⁽¹⁾ The reason for using a noble gold substrate instead of an actively corroding iron substrate is because iron has two phenomena happening simultaneously at the electrode/electrolyte interface—corrosion of iron, which results in mass loss, and adsorption of corrosion inhibitors, which results in mass gain. With the amount of mass expected to be added with molecular adsorption of organic surfactant-type corrosion inhibitors being negligibly small when compared to the mass loss that can happen due to corrosion of substrate, it is fair to use a noble substrate that does not corrode, when the focus is to study adsorption. Otherwise, the mass loss due to corrosion of a steel substrate will overpower any small mass addition due to inhibitor adsorption. Different bulk inhibitor concentrations tested in this study are: 25 ppm(w) [0.5 CMC, 0.0625 mM], 50 ppm(w) [1 CMC, 0.125 mM], and 100 ppm(w) [2 CMC, 0.25 mM] in 1 wt% of NaCl solution prepared using deionized water with the resistivity of 18 $M\Omega \cdot cm$. The concentrations of 25 ppm (w), 50 ppm(w), and 100 ppm(w) are above the surface saturation concentration for the BDA-C14 inhibitor molecule which was established and reported based on electrochemical corrosion rate measurements elsewhere.⁸ Surface saturation concentration is a minimum bulk inhibitor concentration at which the maximum significant decrease in steady-state corrosion rates is achieved.⁷ For example, in Figure 2, the difference in steady-state corrosion rates for bulk inhibitor concentrations of 10 ppm(w), 25 ppm(w), 37.5 ppm(w), and 50 ppm(w) is practically insignificant, hence for this case surface saturation concentration will lie between 5 ppm(w) and 10 ppm(w). The experimental test matrix is shown in Table 1.

2.3 | Quartz Crystal Microbalance with Dissipation Monitoring

The QCM-D unit (Model: X1)⁽¹⁾ used for this study monitors frequency change and dissipation change at multiple overtones simultaneously ($n = 1, 3, 5, 7, 9, 11, \text{ and } 13$).⁵¹ Figure 3 shows the schematic of the QCM-D experimental setup used for inhibitor adsorption experiments. First, a 1 wt% NaCl solution without any inhibitor was pumped through the QCM-D unit cell at a constant flow rate to get a baseline frequency and dissipation response against which any change due to mass adsorption was measured. Then, the valve at the syringe pump was switched to flow the inhibitor solution through the QCM-D unit cell while the change in frequency and dissipation values

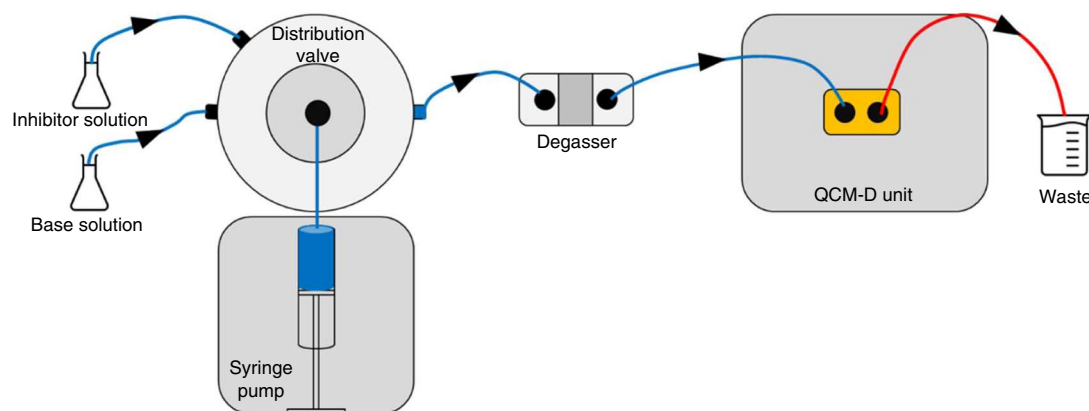


FIGURE 3. Schematic of the QCM-D setup with flow control unit.

⁽¹⁾ purchased from Advanced Wave Sensors S.L. (Paterna, Spain).

were measured with respect to time. The degasser unit as shown in a schematic helped in minimizing the air bubble formation on the surface of the QCR. Measured experimental data are obtained in terms of frequency change and dissipation change at multiple overtones with respect to time.

RESULTS AND DISCUSSION

3.1 | Mass Adsorption and Thickness of the Adsorbed Layer

The adsorption behavior of the BDA-C14 model inhibitor compound was investigated using QCM-D equipped with a flow control unit by measuring a change in resonance frequency and dissipation. In brief, any decrease in resonance frequency would mean the adsorption of molecules on the gold surface and any increase in resonance frequency from a stable value would mean mass being removed, here due to desorption, from the gold-coated QCR if the gravimetric regime of our tool is respected.^{21,33-34} Dissipation in general refers to the mechanical properties of the adsorbed mass or solution properties in the vicinity of the surface. It should be noted that it is a unitless parameter ($\Delta D = \text{energy dissipated/energy stored}$). In theory, for a rigid mass addition such as by electrodeposition

of copper, there is a negligible change in dissipation.^{33,52} But viscoelastic mass adsorption, such as proteins or cells, typically influences the change in dissipation (ΔD) on the order of 10^{-5} to 10^{-4} . Thus, any measured dissipation values less than 10^{-5} can be considered behaving as a rigid mass addition for QCM-D data analysis.³⁶

Measurements at multiple overtones simultaneously enable observation of the frequency and dissipation responses at different wave penetration depths from the substrate surface in the solution. The higher-order overtones have a lower wave penetration depth and measure less of the piezoelectric active area on the QCR.⁵³ At the fundamental mode ($n = 1$) and lower overtones ($n = 3,5$), there is a possibility of interference from the O-ring seal on the QCR in the QCM-D flow cell and, at very high overtones ($n = 13$), the data obtained has more inherent noise. For this reason, the analysis in this research focused on three overtones, $n = 7, 9$, and 11 . Figures 4 through 6 show the experimental results where the measured normalized frequency change ($\Delta f/n$, left y axis) and dissipation change (ΔD , right y axis) are plotted with respect to time (x axis) at the selected overtones ($n = 7, 9$, and 11) for the bulk inhibitor concentrations of 25 ppm(w), 50 ppm(w), and 100 ppm(w), respectively. The scale for dissipation change (ΔD , right y axis) is fixed at $\pm 10^{-4}$

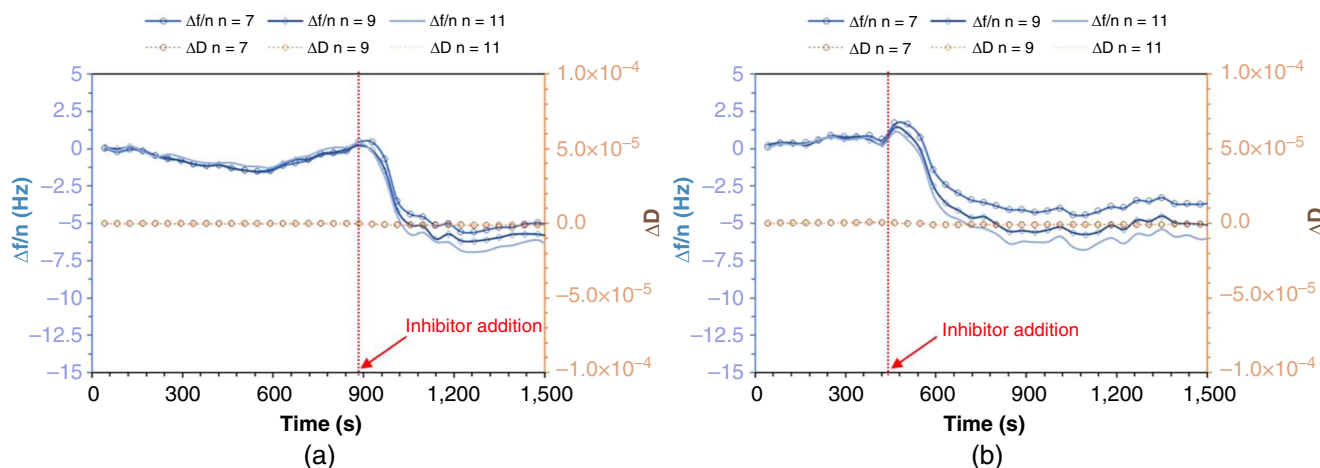


FIGURE 4. Normalized frequency change (in blue shades) and dissipation change (in orange shades) vs. time for inhibitor concentration of 25 ppm(w). (a) and (b) are the results of two experiments.

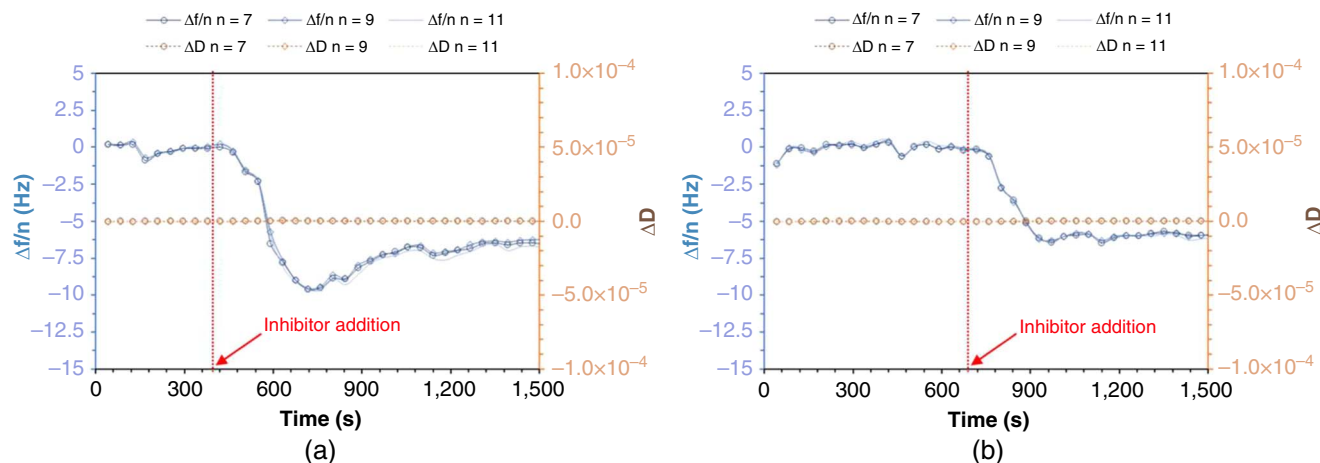


FIGURE 5. Normalized frequency change (in blue shades) and dissipation change (in orange shades) vs. time for inhibitor concentration of 50 ppm(w). (a) and (b) are the results of two experiments.

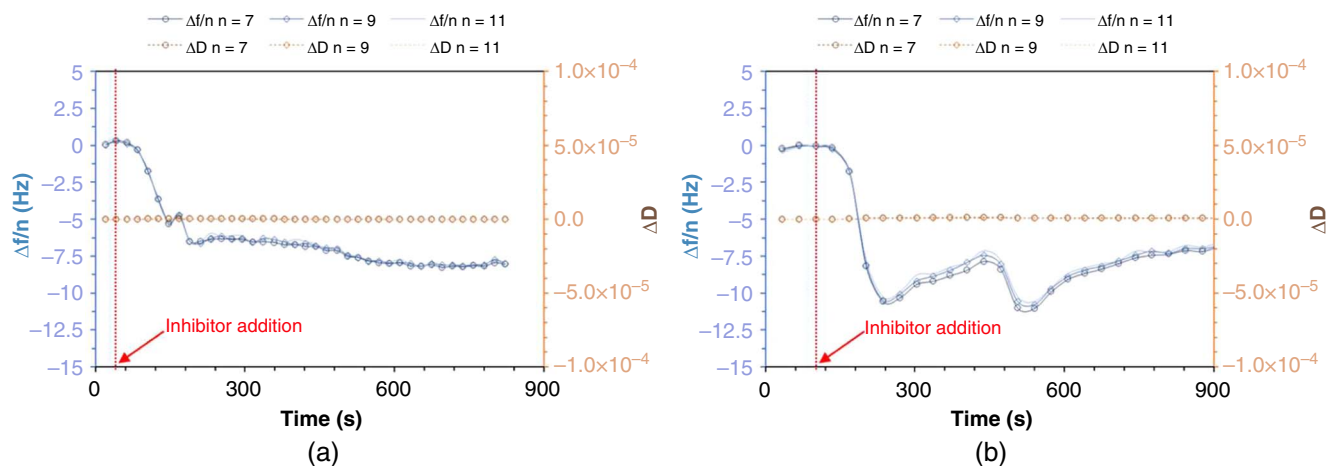


FIGURE 6. Normalized frequency change (in blue shades) and dissipation change (in orange shades) vs. time for inhibitor concentration of 100 ppm(w). (a) and (b) are the results of two experiments.

as any measured dissipation value less than 10^{-5} can be considered as a rigid mass addition.³⁶

A stable baseline in frequency was observed at multiple overtones before the addition of inhibitor molecules against which the change due to inhibitor addition is measured. After the inhibitor solution is pumped through the QCM-D unit, resonance frequency drops with time until it reaches a stable value. This decrease in frequency corresponds to mass adsorption at substrate surface and the final stable value is indicative of a dynamic equilibrium where adsorption and desorption rates become equal. Moreover, the normalized frequency change overlaps at multiple overtones indicating that the adsorbed mass behaves as a rigid mass as compared to a bulk solution.³⁶

The dissipation change measured for all of the tested concentrations is of the order of 10^{-8} to 10^{-6} , which looks close to zero when plotted in the realm of viscoelastic mass addition, $\Delta D > 10^{-4}$.³⁶ So, it was confirmed that the adsorbed mass can be reasonably assumed to behave as a rigid mass for data analysis. In a previous publication, with results analysis for 50 ppm(w) and 100 ppm(w) bulk inhibitor concentrations, a small load approximation (SLA) model was used to analyze the measured frequency change and dissipation change simultaneously.³⁷ A shear wave is generated due to oscillations of QCR perpendicular to the QCR surface and into the bulk solution. SLA model is based on solving the wave equation at different interfaces involved such as gold substrate/adsorbed inhibitor layer interface and adsorbed inhibitor layer/bulk solution interface in the experimental system.^{38,54} Using the SLA model, it was established with a high degree of confidence that the adsorbed layer was behaving as rigid at those experimental conditions. More precisely, this adsorbed layer behaved as a rigid mass when compared with the ambient bulk liquid. Please note that, for SLA analysis, an independent input of physical density is a required input which was taken as $1,000 \text{ kg/m}^3$ in that case. This assumption was discussed in a previous publication³⁷ and more supporting arguments are added in the present paper later in the *Discussion* section.

Figure 7 compares the mass change per unit area estimated using Sauerbrey's equation, Equation (1), and the SLA model for different bulk inhibitor concentrations. With almost equal values determined by the two methods, this suggests that the rigid mass assumption made for Sauerbrey's analysis is reasonable because there was no such assumption made for SLA analysis.³⁷ Hence, the necessary conditions to use Sauerbrey's

equation are fulfilled and Table 2 summarizes the adsorbed mass per unit area calculated using Sauerbrey's equation.^{21,34}

$$\frac{\Delta m}{A} = - \left(\frac{\Delta f}{n} \right) \left(\frac{C_f}{C_f} \right) \quad (1)$$

Where Δf is change in resonance frequency measured using QCM-D, Hz; n is the number of overtones; A is piezoelectrically active area, cm^2 ; and C_f for 5 MHz AT-cut quartz crystal in air is $56.6 \text{ Hz} \cdot \mu\text{g}^{-1} \cdot \text{cm}^2$.

Knowing the adsorbed mass per unit area, the averaged thickness of the adsorbed layer can be estimated if the density of the adsorbed layer is known, Equation (2). The use of $1,000 \text{ kg/m}^3$ is often assumed as a reasonable value for the physical density of adsorbed layers in bulk aqueous phase solutions.^{38,54-55} The adsorbed layer density of $1,000 \text{ kg/m}^3$ for the experimental system presented in this research was also verified by the analysis of the molecular simulation results reported by Singh, et al., for surfactant type molecules in bulk aqueous phase.⁴⁹ With assistance from the authors, adsorbed

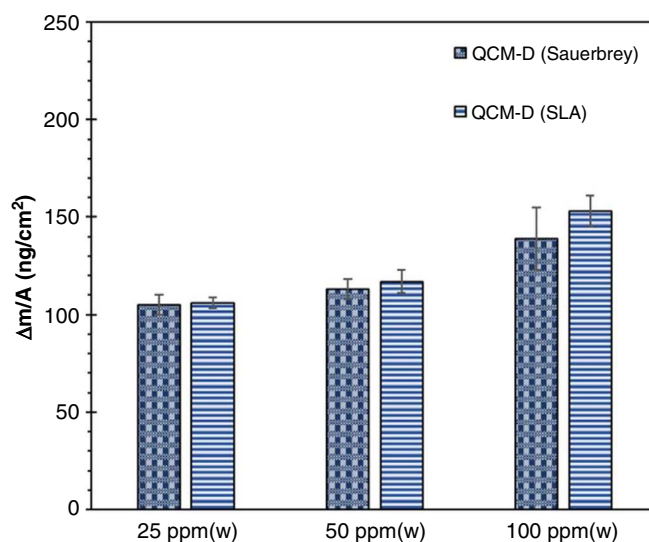


FIGURE 7. Comparison of adsorbed mass estimated using Sauerbrey's equation and SLA model³⁷ for adsorption of BDA-C14 on gold-coated QCR.

Table 2. Results Summary for Inhibitor Adsorption Experiments

Parameter	Average value		
	25 ppm(w)	50 ppm(w)	100 ppm(w)
$\Delta f/n$ (Hz)	5.8±0.3	6.4±0.3	7.9±0.9
$\Delta m/A$ (ng/cm ²)	105±5	113±5	139±16
Average adsorbed layer thickness (nm)	1.05±0.05	1.13±0.05	1.39±0.16

layer density for two model inhibitor compounds: quat-12 (functional head group—dimethylbenzylammonium and alkyl tail comprising 12 carbon atoms (-C₁₂H₂₅)) and decanthal (functional head group—thiol (-SH) and alkyl tail comprising 10 carbon atoms (-C₁₀H₂₁)), were calculated to be 1,100 kg/m³ and 960 kg/m³, respectively. Please note that the quat-12 molecule has the same functional head group as the BDA-C14 model inhibitor compound used in this study with the only difference being in the alkyl tail length. This analysis is based on density profiles presented by authors in Figures 2, 5, and 8 of the publication.⁴⁹ The base area of the simulation box was known to be 49.04 Å × 49.97 Å and adsorbed layer thickness was taken to be 22 Å for quat-12 and 25 Å for decanthal molecules as reported.⁴⁹ Having the total volumetric area and knowing the total number of species in the volume—30 quat-12 molecules, 1,381 water molecules, and 27 bromide ions for quat-12 case and 196 decanthal molecules for decanthal case; adsorbed layer densities were estimated for each case. These calculations further support the use of adsorbed layer density to be 1,000 kg/m³ in the present experimental system of BDA-C14 molecules in the aqueous solution. Calculated values of the averaged adsorbed layer thickness are also reported in Table 2.

$$\text{Average adsorbed layer thickness} = \left(\frac{\frac{\Delta m}{A}}{\text{density of adsorbed layer}} \right) \quad (2)$$

In a separate study conducted using atomic force microscopy (AFM), Wang, et al., reported the thickness of adsorbed

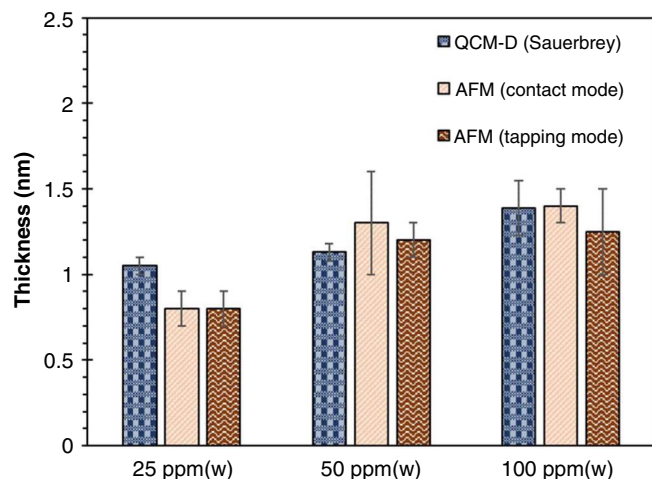


FIGURE 8. Comparison of average adsorbed layer thickness estimated using QCM-D and reported by Wang, et al., for measurements with AFM¹⁴ for adsorption of BDA-C14 on noble substrates, gold for QCM-D and mica for AFM.

layer for the same BDA-C14 model compound on a mica substrate, which is also a noble substrate.¹⁴ Figure 8 compares the results of adsorbed layer thickness measured using QCM-D with previously reported values from AFM measurements, using both contact mode and tapping mode. AFM measurements are physical measurements of the adsorbed layer thickness so there is no assumption associated with the adsorbed layer density of 1,000 kg/m³. These previously reported values match very well with the adsorbed layer thickness estimated using QCM-D measurements.

This discussion of AFM measurements and molecular simulation results reported by different researchers supports the two assumptions made for QCM-D analysis—that the adsorbed layer behaves as a rigid mass deposit and adsorbed layer density can reasonably be assumed as 1,000 kg/m³.

3.2 | Quantification of Kinetics of the Inhibitor Adsorption Process

Using the validity of Sauerbrey's analysis for QCM-D results, a similar line of reasoning can be extended to each measured data point in the frequency change curves (Figures 4 through 6) by converting the variation in frequency to a variation of adsorbed mass per unit area vs. time using Equation (1). An example of conversion from data in Figure 5(a) is shown in Figure 9.

The methodology used to quantify the kinetics of the adsorption process is described below.

- Following the "geometric blockage" model,⁵⁶ the governing equation to link mass change and surface coverage can be derived as follows

$$\frac{\Delta m}{A} \propto \text{Surface Coverage} (\theta) \quad (3)$$

Integrating the above equation gives

$$\frac{\Delta m}{A} = c_1 \theta + c_2 \quad (4)$$

where c_1 and c_2 are integration constants. At the start of the experiment, when there is no mass change ($\frac{\Delta m}{A} = 0$) and surface coverage, $\theta = 0$; which gives $c_2 = 0$. Hence, the governing equation is

$$\frac{\Delta m}{A} = c_1 \theta \quad (5)$$

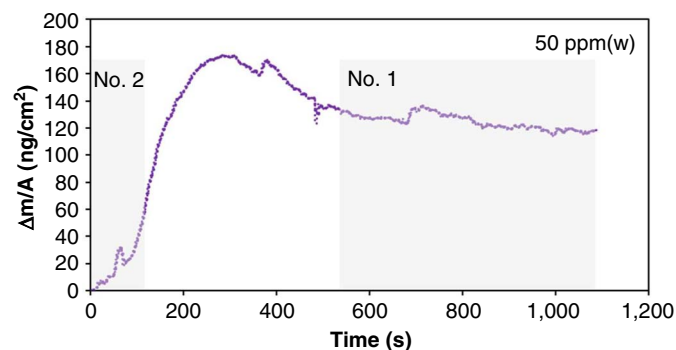


FIGURE 9. Adsorbed mass per unit area versus time derived from frequency change versus time using Sauerbrey's equation. No. 1 represents equilibrium adsorption and no. 2 represents a condition corresponding to no inhibitor coverage as time approaches zero.

c_1 is a constant that corresponds to an adsorbed mass at maximum (100%) geometrical coverage. The next step is to estimate the value of c_1 .

2. Assuming a Langmuir adsorption isotherm

$$\frac{d\theta}{dt} = k_A C_{inh}(1 - \theta) - k_D \theta \quad (6)$$

where C_{inh} is bulk inhibitor concentration, k_A and k_D are adsorption and desorption kinetic constants, respectively. For boundary condition no. 1, when $\theta \rightarrow \theta_{eq}$, $\frac{d\theta}{dt} = 0$, Equation (6) becomes

$$0 = k_A C_{inh}(1 - \theta) - k_D \theta \quad (7)$$

Combining Equations (5) and (7) and using $K_{AD} = \frac{k_A}{k_D}$ where K_{AD} is the equilibrium constant, gives

$$\frac{\Delta m}{A} = c_1 \frac{K_{AD} C_{inh}}{1 + K_{AD} C_{inh}} \quad (8)$$

By fitting equilibrium mass per unit area given in Table 2 with Equation (8), the two unknowns parameters can be estimated, $K_{AD} = 32.2 \text{ mM}^{-1}$ and $c_1 = 151 \text{ ng/cm}^2$. The equilibrium surface coverage (θ_{eq}) at different bulk inhibitor concentrations tested in this study were then calculated from c_1 using Equation (9) and are shown in Table 3.

$$\theta_{eq} = \frac{\left(\frac{\Delta m}{A}\right)}{c_1} \quad (9)$$

For boundary condition no. 2, when $t \rightarrow 0$, $\theta \rightarrow 0$, Equation (6) becomes

$$\frac{d\theta}{dt} = k_A C_{inh} \quad (10)$$

Combining Equation (10) with Equation (5) gives

$$\frac{d(\Delta m/A)}{dt} = c_1 k_A C_{inh} \quad (11)$$

Solving Equation (11) for all of the different bulk inhibitor concentrations tested gives $k_A = 0.075 \pm 0.02 \text{ mM}^{-1} \cdot \text{s}^{-1}$ and using the value of K_{AD} , determined earlier, k_D was calculated to be $0.0023 \pm 0.0007 \text{ s}^{-1}$.

It should be noted here that the surface saturation concentration for BDA-C14 inhibitor molecules was established using electrochemical corrosion rate measurements in the range of 5 ppm(w) to 10 ppm(w).⁸ However, for QCM-D measurements at bulk inhibitor concentrations above the surface saturation concentration, the calculated geometrical surface coverage did not reach 100% (Table 3). This indicates that maximum protection for each inhibitor concentration with respect to corrosion can be achieved even when inhibitor

Table 3. Equilibrium Surface Coverage Estimated Using QCM-D for Adsorption of BDA-C14 on Gold-Coated QCR

Parameter	25 ppm(w)	50 ppm(w)	100 ppm(w)
θ_{eq}	0.69	0.74	0.91

molecules may not be covering the entire geometrical area of the electrode. Traditionally, the corrosion inhibition efficiency at a steady state is used as a measure of inhibitor surface coverage. However, QCM-D measurements and analysis reveal that this assumption is not accurate. QCM-D results are further supported by the presence of holes in the adsorbed layer of BDA-C14 molecules as shown by AFM explorations reported by Wang, et al. It suggests that the adsorbed BDA-C14 molecules are not always in a well-defined monolayer covering the entire metal surface.¹⁴

3.3 | Discussion on the Possible Configurations of the Adsorbed Layer at 100% Geometrical Coverage

If a Langmuir adsorption isotherm is assumed to be valid for this experimental scenario, c_1 corresponds to the adsorbed mass at the maximum (100%) geometrical coverage. As part of the adsorption kinetics quantification, c_1 was estimated to be 151 ng/cm^2 . In this section, some theoretical calculations of the extreme cases are performed to delve deeper into the possible adsorbed layer configurations. These calculations are done using the projected area on the substrate surface of one molecule (accounting for molecular repulsions) as per the chosen configuration and then calculating the mass density of the close-packed adsorbed layer for that configuration.

Case 1: Assembled monolayer in lying down configuration, Figure 10(a); mass density of one packed layer is approximately 36 ng/cm^2 .

Case 2: Assembled bilayer in lying down configuration, Figure 10(b); mass density of one packed layer is approximately 49 ng/cm^2 .

Case 3: Assembled monolayer in standing-up configuration, Figure 10(c); mass density of one packed layer is approximately 90.5 ng/cm^2 .

Case 4: Assembled bilayer in standing-up configuration, Figure 10(d); mass density of one packed layer is approximately 181 ng/cm^2 .

The mass density for an assembled bilayer in standing-up configuration has the closest value to the estimated c_1 . Moreover, in this configuration, the adsorbed layer thickness corresponds to the molecular length of BDA-C14, which is approximately 1.9 nm .¹⁴ Hence, for a calculated adsorbed layer thickness between 1 nm and 1.4 nm , it can be reasonably assumed that the predominant configuration of inhibitor molecules for the QCM-D measured adsorbed layer is in some sort of a tilted assembled bilayer configuration (Figure 11), which is again consistent with the results reported for BDA-C14 using AFM measurements and molecular simulations in separate studies.^{14,45} Please note that, in reality, there can be a mix of all the extreme scenarios discussed above as well as other possible configurations and it is not possible to see the molecular orientations using QCM-D. However, this is a modest attempt to shed light on various possibilities and to introduce a methodology for the community to use and advance the utilization of QCM-D for this application.

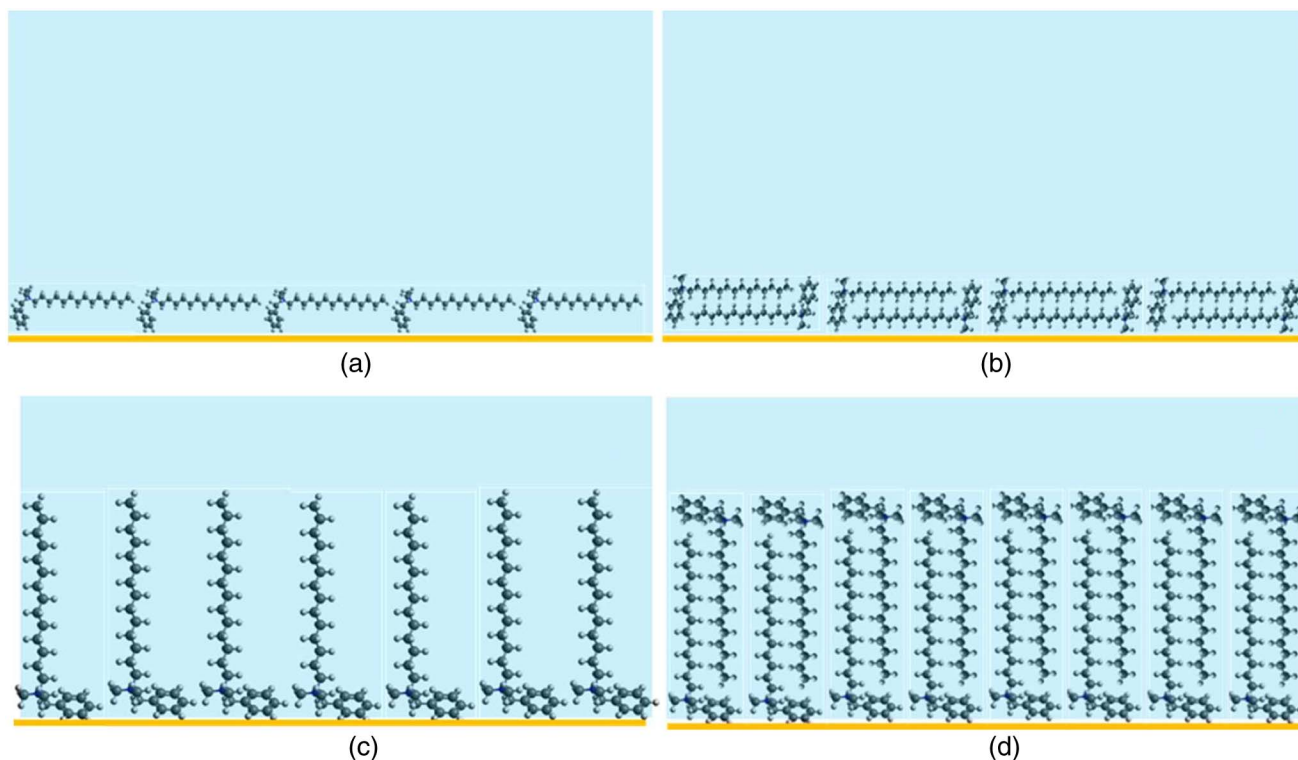


FIGURE 10. Possible adsorbed inhibitor molecule layer configurations for BDA-C14.

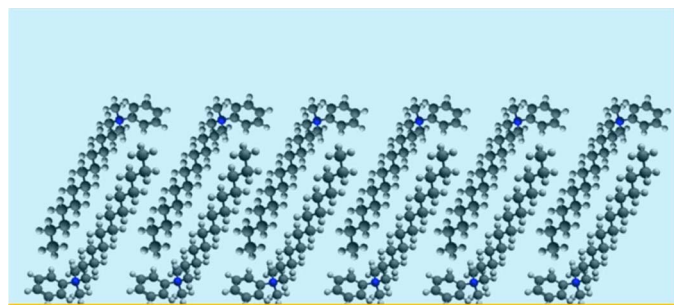


FIGURE 11. Schematic showing tilted bilayer configuration of adsorbed BDA-C14 molecules on gold.

CONCLUSIONS

In this research, QCM-D experiments were performed on gold electrode to characterize the adsorption behavior of a model inhibitor compound, BDA-C14, at various bulk inhibitor concentrations. The findings from these experiments alongside theoretical calculations led to the following conclusions:

➤ Adsorbed layer properties

- i. The dissipation change observed due to adsorbed layer at different bulk inhibitor concentrations is small (in the order of 10^{-8} to 10^{-6}), indicating the negligible viscoelastic losses due to interaction of the adsorbed layer with aqueous solution. This suggests that the adsorbed inhibitor layer behaves as a rigid mass, which validates the use of Sauerbrey's analysis for the measured QCM-D data.
- ii. At bulk inhibitor concentrations of 25 ppm(w), 50 ppm(w), and 100 ppm(w), the average adsorbed layer thickness estimated using QCM-D measurements lie in the range of 1 nm to 1.4 nm.

Based on this averaged adsorbed layer thickness and theoretical calculations of mass per unit area for various extreme configuration cases, adsorbed inhibitor molecules can be reasonably assumed to be arranged in a tilted bilayer configuration.

➤ Quantification of kinetics of the inhibitor adsorption process

- i. Bulk inhibitor concentrations above the surface saturation, as reported from previously published corrosion inhibition experiments, the results in equilibrium geometrical surface coverage was less than 100%, as determined using QCM-D.
- ii. The adsorption and desorption kinetic constants for the BDA-C14 model inhibitor compound were determined, with a comprehensive methodology provided.

ACKNOWLEDGMENTS

The author would like to thank the following companies for their financial support: Ansys, Baker Hughes, ChampionX LLC, Chevron Energy Technology, Clariant Corporation, Conoco-Phillips, ExxonMobil, M-I SWACO (SLB), Multi-Chem (Halliburton), Occidental Oil Company, Pertamina, Saudi Aramco, Shell Global Solutions, and TotalEnergies. The authors would also like to thank Dr. David Young for synthesizing and characterizing the model inhibitor compound used in this work. The authors sincerely acknowledge Dr. Sumit Sharma and Dr. Himanshu Singh for their inputs about the calculation of adsorbed layer densities reported in their published work.

References

1. M.G. Fontana, *Corrosion Engineering*, 3rd ed. (New Delhi, India: Tata Mc Graw Hill Education Private Limited, 2005), p. 282.

2. E. McCafferty, *Introduction to Corrosion Science* (New York, NY: Springer 2010), p. 357.
3. V.S. Sastri, *Green Corrosion Inhibitors: Theory and Practice* (New York, NY: John Wiley & Sons, Inc., 2011).
4. Z. Belarbi, F. Farelas, M. Singer, S. Nešić, *Corrosion* 72 (2016): p. 1300-1310.
5. V. Pandarinathan, K. Lepková, S.I. Bailey, T. Becker, R. Gubner, *Ind. Eng. Chem. Res.* 53 (2014): p. 5858-5865.
6. Y. Zhu, M.L. Free, R. Woollam, W. Durnie, *Prog. Mater. Sci.* 90 (2017): p. 159-223.
7. N. Moradighadi, S. Lewis, J.D. Olivo, D. Young, B. Brown, S. Nešić, *Corrosion* 77 (2021): p. 266-275.
8. K. Singla, B. Brown, S. Nešić, *Corrosion* 80 (2024): p. 603-607.
9. J.M. Domínguez Olivo, B. Brown, S. Nešić, "Modeling of Corrosion Mechanisms in the Presence of Quaternary Ammonium Chloride and Imidazoline Corrosion Inhibitors," CORROSION 2016, paper no. 7406 (Houston, TX: NACE, 2016).
10. J.M. Domínguez Olivo, B. Brown, D. Young, S. Nešić, "Electrochemical Model of CO₂ Corrosion in the Presence of Quaternary Ammonium Corrosion Inhibitor Model Compounds," CORROSION 2019, paper no. 13392 (Houston, TX: NACE, 2019).
11. R.C. Woolam, J. Owen, Y. Hayatgheib, R. Barker, "Corrosion Inhibitor Surfactant Optimization: Part 2—Adsorption Kinetics Approach," CORROSION 2022, paper No. 18045 (Houston, TX: AMPP, 2022).
12. W.J. Lorenz, F. Mansfeld, *Electrochim. Acta* 31 (1986): p. 467-476.
13. M.A. Veloz, I.G. Martínez, *Corrosion* 62 (2006): p. 283-292.
14. H. Wang, S. Sharma, A. Paillet, B. Brown, S. Nešić, *Corrosion* 78 (2022): p. 990-1002.
15. J.D. Olivo, B. Brown, D. Young, S. Nešić, *Corrosion* 75 (2018): p. 137-139.
16. J.M. Domínguez Olivo, D. Young, B. Brown, S. Nešić, "Effect of Corrosion Inhibitor Alkyl Tail Length on the Electrochemical Process Underlying CO₂ Corrosion of Mild Steel," CORROSION 2018, paper no. 11537 (Houston, TX: NACE, 2018).
17. R.C. Woolam, J. Owen, Y. Hayatgheib, R. Barker, "Corrosion Inhibitor Surfactant Optimization: Part 1—Inhibitor Efficiency," CORROSION 2022, paper No. 18043 (Houston, TX: AMPP, 2022).
18. A. Chandra, W. Durnie, J. Vera, R. Woolam, "Relationship between Inhibitor Adsorption and Surfactant Properties: Part II—Critical Parameters," CORROSION 2019, paper no. 13245 (Houston, TX: NACE, 2019).
19. Y. Zhu, M.L. Free, G. Yi, *Corros. Sci.* 102 (2016): p. 233-250
20. Y. He, S. Ren, X. Wang, D. Young, M. Singer, Z. Belarbi, M. Mohamed-Said, S. Camperos, M.R. Khan, K. Cimatu, *Corrosion* 78 (2022): p. 625-633.
21. M. Hepel, "Electrode-Solution Interface Studied with Electrochemical Quartz Crystal Nanobalance," *Interfacial Electrochemistry Theory: Experiment and Applications*, 1st ed. (New York, NY: Taylor and Francis Group, 1999), p. 599-630.
22. Y. Ding, Mechanistic Understanding of CO₂ Corrosion Inhibition at Elevated Temperatures (Doctoral Dissertation, Ohio University, 2019), p. 67.
23. D.S. Karpovich, G.J. Blanchard, *Langmuir* 10 (1994): p. 3315-3322.
24. D.S. Karpovich, G.J. Blanchard, *J. Chem. Educ.* 72 (1995): p. 466.
25. M.A. Petrunin, L.B. Maksiyeva, T.A. Yurasova, E. V. Terekhova, M.A. Maleeva, V.A. Kotenev, E.N. Kablov, A.Yu. Tsvadze, *Protect. Met. Phys. Chem. Surf.* 51 (2015): p. 1010-1017.
26. G. Vastag, A. Shaban, M. Vraneš, A. Tot, S. Belić, S. Gadžurić, *J. Mol. Liq.* 264 (2018): p. 526-533.
27. C. Wang, S. Zanna, I. Frateur, B. Despax, P. Raynaud, M. Mercier-Bonin, P. Marcus, *Surf. Coat. Technol.* 307 (2016): p. 1-8.
28. B.B. Berkes, G. Inzelt, E. Vass, *Electrochim. Acta* 96 (2013): p. 51-60.
29. Yu.I. Kuznetsov, L.B. Maksiyeva, M.A. Petrunin, N.P. Andreeva, *Russ. J. Electrochem.* 45 (2009): p. 1240-1244.
30. I. Jevremović, M. Singer, S. Nešić, V. Mišković-Stanković, *Corros. Sci.* 77 (2013): p. 265-272.
31. K.W. Hipps, A. Bhattarai, "Measuring Desorption Rates From Self-Assembled Monolayers at the Solution-Solid Interface," in *Encyclopedia of Interfacial Chemistry*, ed. K. Wandelt (Oxford, United Kingdom: Elsevier, 2018), p. 100-109.
32. R. Lalauze, "Adsorption Phenomena," in *Chemical Sensors and Biosensors*, ed. R. Lalauze (Hoboken, NJ: John Wiley & Sons, Ltd, 2012), p. 27-47.
33. K. Singla, H. Perrot, O. Sel, B. Brown, S. Nesić, "Use of Quartz Crystal Microbalance in Study of Inhibitor Adsorption," VIRTUAL CORROSION, paper no. 16653 (Houston, TX: AMPP, 2021).
34. G. Sauerbrey, *Z. Phys.* 155 (1959): p. 206-222.
35. M.R. Deakin, D.A. Buttry, *Anal. Chem.* 61 (1989): p. 1147A-1154A.
36. M.C. Dixon, *J. Biomol. Tech.* 19 (2008): p. 151.
37. K. Singla, H. Perrot, B. Brown, S. Nesić, "Adsorption of Model Inhibitor Compound Characterized Using Quartz Crystal Microbalance with Dissipation Monitoring," CORROSION 2023, paper no. 19145 (Houston, TX: AMPP, 2023).
38. D. Johannsmann, *Phys. Chem. Chem. Phys.* 10 (2008): p. 4516-4534.
39. J.T. Woodward, I. Doudevski, H.D. Sikes, D.K. Schwartz, *J. Phys. Chem. B* 101 (1997): p. 7535-7541.
40. M. Jaschke, H.-J. Butt, H.E. Gaub, S. Manne, *Langmuir* 13 (1997): p. 1381-1384.
41. G.E. Poirier, E.D. Pylant, *Science* 272 (1996): p. 1145-1148.
42. H.N. Patrick, G.G. Warr, S. Manne, I.A. Aksay, *Langmuir* 15 (1999): p. 1685-1692.
43. S. Manne, T.E. Schäffer, Q. Huo, P.K. Hansma, D.E. Morse, G.D. Stucky, I.A. Aksay, *Langmuir* 13 (1997): p. 6382-6387.
44. D. Johannsmann, "Combined Instruments," in *The Quartz Crystal Microbalance in Soft Matter Research: Fundamentals and Modeling*, ed. D. Johannsmann (Cham, Switzerland: Springer International Publishing, 2015), p. 359-376.
45. S. Sharma, H. Singh, X. Ko, *J. Phys. Chem. B* 123 (2019): p. 7464-7470.
46. H. Singh, S. Sharma, *Mol. Simul.* 47 (2021): p. 420-427.
47. S. Sharma, X. Ko, Y. Kurapati, H. Singh, S. Nešić, *Corrosion* 75 (2018): p. 90-105.
48. X. Ko, S. Sharma, *J. Phys. Chem. B* 121 (2017): p. 10364-10370.
49. H. Singh, S. Sharma, *J. Chem. Theory Comput.* 18 (2022): p. 2513-2520.
50. M.D. Hanwell, D.E. Curtis, D.C. Lonie, T. Vandermeersch, E. Zurek, G.R. Hutchison, *J. Cheminform.* 4 (2012): p. 17.
51. Y.J. Montagut, J. V. García, Y. Jiménez, C. March, A. Montoya, A. Arnau, *Rev. Sci. Instrum.* 82 (2011): p. 064702.
52. C. Gabrielli, M. Keddad, R. Torresi, *J. Electrochem. Soc.* 138 (1991): p. 2657.
53. A. Arnau, Y. Montagut, J. V. García, Y. Jiménez, *Meas. Sci. Technol.* 20 (2009): p. 124004.
54. D. Johannsmann, *The Quartz Crystal Microbalance in Soft Matter Research*, 1st ed. (Cham, Switzerland: Springer Cham, 2015).
55. D. Johannsmann, W. Bucking, B. Bode, J. Petri, "Simple Frequency-Based Sensing of Viscosity and Dielectric Properties of a Liquid Using Acoustic Resonators," in 2009 IEEE International Frequency Control Symposium Joint with the 22nd European Frequency and Time Forum (2009), p. 855-860.
56. T. Murakawa, S. Nagaura, N. Hackerman, *Corros. Sci.* 7 (1967): p. 79-89.